1
2
3
4
5
6
7

Sound transmission across a narrow sidebranch array duct muffler at low Mach number

H.M.Yu and S.K.Tang[a]

Department of Building Services Engineering
The Hong Kong Polytechnic University
Hong Kong
China

[a]Corresponding author
 Email address : shiu-keung.tang@polyu.edu.hk

Abstract

The sound transmission loss across a duct muffler in the form of a linear array of eleven narrow sidebranches is examined experimentally in the present study. The introduction of a low Mach number duct flow deteriorates the broadband acoustical performance of the muffler and strong sound transmission loss dips and sound amplifications are observed at high flow speeds. It is found that a stronger acoustic pressure magnitude inside the sidebranches improves the muffler's performance in the presence of the duct flow. A theoretical analysis using a two-sidebranch array muffler is conducted and the results indicate the possibility of increasing the sound pressures inside the sidebranches by locating the shorter sidebranch upstream of the longer one. The results of further experiments validate the theoretical deduction. They also confirm that the muffler with sidebranches arranged in the order of decreasing acoustic impedance magnitude has stronger resilience against aerodynamic disturbance and gives better performance when the upstream excitation level and the duct flow speed are fixed.

I. INTRODUCTION

The attenuation of noise from the air conditioning and ventilation systems has long been a challenging problem in heavily serviced modern buildings nowadays.[1] The noise from the air handling units propagates into the interior occupied zones through the ductwork, and it has to be attenuated satisfactorily so as to create an acceptable indoor acoustical environment for the well-being of the occupants.[2] Flow duct silencers have attracted the attention of researchers and engineers for decades, but the quest for better broadband silencing devices with lower static pressure loss remains a hot topic.

Dissipative silencers, which are installed with fibrous porous materials to dissipate sound energy into heat, are the traditional flow duct noise mitigation devices.[3] However, this kind of silencers does suffer from many drawbacks. The major drawback is that the significant static pressure drop across such a silencer leads to over-design and unnecessary fan power consumption. Silencers of this kind are also not applicable to areas where a stringent hygienic condition is required or where the air is dirty/greasy. Detailed discussions on these drawbacks have been given in Tang[4] and thus they are not repeated here. Silencers adopting flexible or perforated panels[5,6] or active control[7] also suffer from similar problems.

Passive reactive devices are interesting alternatives as they usually result in much less static pressure drop. Typical examples include the Helmholtz resonators,[8] plenum chambers,[9] Herschel-Quincke tubes,[10] quarter-wavelength tubes[11] and there are many derivatives as illustrated in Munjal.[12] Tang and Tang[13] examined the strong noise reduction characteristics of coupled duct cavities and more recently, Jena and Qiu[14] presented a metamaterial approach for duct silencing. However, reactive silencers are usually narrow-band devices. Therefore, there have been much effort in constructing broadband reactive silencers, among which the use of coupled resonators and sidebranches are being actively investigated.

For the resonators, Griffin et al.[15] showed the presence of multiple sound transmission loss spectral peaks when two resonators are coupled together through a duct and a sharable sidewall. Seo

and Kim[16] showed that broadband sound transmission loss in a duct can be achieved by coupling four wall-mounted resonators of the right resonance frequency ratios. Howard et al.[17] illustrated that broadband sound transmission loss can also be resulted by packing together many small resonators of different resonance frequencies in a ducted condition.

The resonance of a sidebranch flush mounted on a duct wall results in strong but narrow band sound transmission loss as shown in Howard et al.[11] Tang[4] showed that the closely packed sidebranches of different lengths can give rise to broadband sound transmission loss. Červenka and Bednařík[18] optimized the broadband sound transmission loss of coupled sidebranches by considering the lengths of and the separations between sidebranches in the absence of a duct flow.

However, though the working bandwidths of such reactive devices can successfully be broadened using coupling method, the shear layer separation at the mouths of these devices and the subsequent aeroacoustical activities in the presence of a low Mach number duct flow have limited their performance. A good example is the observation of Tonon et al.[19] which shows strong aeroacoustic radiation when the resonating air fluctuations inside their tubes coupled with the shear layers at the tube mouths. Also, Nelson et al.[20] demonstrated experimentally that the shear layer at the mouth of a resonator can lead to very strong acoustic radiation if its oscillation locks on with that of the resonator. The observed reduction of the sound transmission loss across a resonator in the presence of a low Mach number duct flow by Tang[21] suggests also the presence of flow induced noise. Such phenomenon is again observed in the numerical results of Pan et al.[22] on two coupled resonators with a perforated sharable sidewall. Pan et al.[22] also illustrated that the direction of air flow can affect the sound transmission across these resonators. However, the underlying physical mechanism for this effect has not been discussed.

The narrow sidebranch array mufflers of Tang and his co-worker[4,23] can give a broadband noise reduction and has great application potential. However, their performance under the influence of a low Mach number duct flow is unclear. As inferred from the numerical results of Pan et al.,[22] the direction of the duct flow could affect the performances of the mufflers. A series of experiments
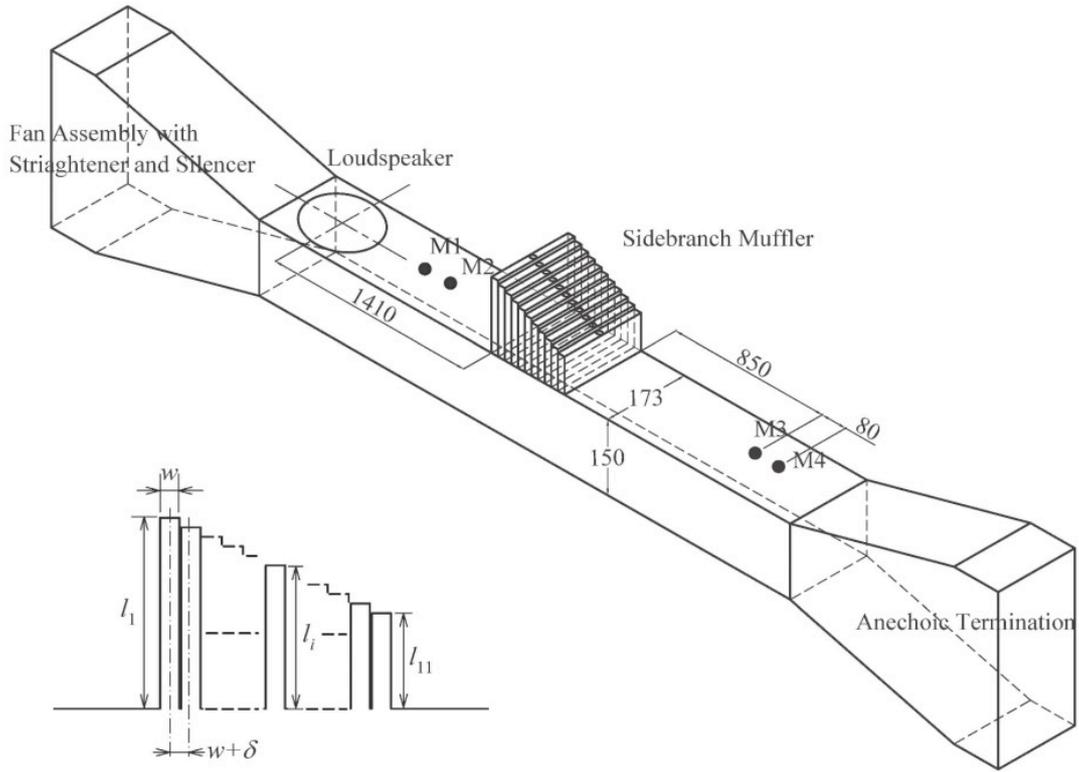
FIG. 1 Schematics of the experimental setup and cross-section of sidebranch muffler.
All dimensions in mm.

1   is derived in the present study to quantify the corresponding sound transmission losses across these

2   mufflers. Effort is also made on deriving a method to reduce the aerodynamic influence on the

3   mufflers' performance.

4

5   **II. EXPERIMENTAL SETUP**

6   Figure 1 shows the schematics of the test rig and the muffler adopted in the present study.

7   The test rig consisted of a quiet flow facility with a converging section, a test section where the

8   narrow sidebranch array muffler was installed, a 6-inch aperture loudspeaker and an anechoic

9   termination designed according to Neise et al.[24] The sound power reflection coefficient due to this

10   termination was less than 0.01 at frequencies above 200 Hz,[25] which covers the frequency range of

11   interest in the present study. The duct height, a, and the duct spanwise width, b, of the test section

12   are 150 mm and 173 mm respectively. The upper frequency bound in the foregoing analysis is set at

1 850 Hz as the first higher spanwise mode cut-on frequency of the duct is ~990 Hz. White noise was

2 fed to the loudspeaker during the experiment.

3 The muffler in this study was made of stainless steel. It consisted of 11 sidebranches of

4 different lengths but the same width, w, of 15 mm ($0.1a$). The thickness of the wall between adjacent

5 sidebranches, δ, was 1.5 mm ($0.01a$). There was a hole at the rigid end of each sidebranch for

6 mounting microphone or inserting pressure transducer into the sidebranch. These holes were rigidly

7 filled up and kept air tight during measurement. The lengths of the longest and shortest sidebranch

8 in the array, l_1 and l_{11}, were 150 mm and 75 mm respectively.

9 There are two sidebranch length arrangements suggested by Tang.[4] One is in the form of a

10 linear variation (LL) such that the length of the ith sidebranch, l_i, is

$$l_i = l_1 - 0.1(i-1)(l_1 - l_{11}).\tag{1a}$$

12 The other one is established based on an approximately linear variation of fundamental resonance

13 frequency of the sidebranch (LF) :

$$\frac{1}{l_i} = \frac{1}{l_1} + 0.1(i-1)\left(\frac{1}{l_{11}} - \frac{1}{l_1}\right).\tag{1b}$$

15 Both of these sidebranch mufflers were tested in the present study. Table I gives the length of each

16 sidebranch and the corresponding fundamental resonance frequency $k_{i,res}a$ obtained by experiment

17 using the present duct and with other sidebranch mouths rigidly closed.

18 The sound transmission losses across the mufflers were measured in the present study using

19 the four-microphone method,[25] which is established based on the two-microphone method of Chung

20 and Blaser.[26] Two pairs of Brüel & Kjær Type 4935 microphones, M1/M2 and M3/M4, each located

Table I. Lengths of sidebranches and their fundamental resonance frequencies.

i	LF Muffler		LL Muffler	
	l_i/a	$k_{i,res}a/\pi$	l_i/a	$k_{i,res}a/\pi$
1	1.0000	0.4609	1.0000	0.4609
2	0.9093	0.5020	0.9500	0.4810
3	0.8333	0.5431	0.9000	0.5073
4	0.7693	0.5825	0.8500	0.5318
5	0.7140	0.6201	0.8000	0.5633
6	0.6667	0.6595	0.7500	0.5956
7	0.6253	0.6953	0.7000	0.6324
8	0.5880	0.7294	0.6500	0.6735
9	0.5553	0.7636	0.6000	0.7190
10	0.5267	0.7942	0.5500	0.7697
11	0.5000	0.8257	0.5000	0.8257

far away on one side of the test section, were used to measure the incident and transmitted waves. Evanescent waves should have significantly attenuated before reaching these microphones. Following the recommendation of Åbom and Bodén[27] and the frequency range of the present study, the separation between microphones within each microphone pair was fixed at 80 mm. The formulation of the calculation procedure can be found in Tang and Li[26] and thus it is not repeated here.

A pressure transducer P (Endevco 8507C-2 with Model 136 amplifier) was used to measure the pressure signals along the length of each sidebranch simultaneously with the sound transmission loss measurement. In order to understand the magnitude of the pressure inside the sidebranch, the transfer functions between the pressure transducer signals and the incident sound wave (I), $H_{P,I}$, will be presented in the foregoing analysis instead the actual acoustic pressures in Pa. The latter is also not preferred as its spectral characteristics are dictated by the loudspeaker. The calculation of $H_{P,I}$ was done based on the two-microphone procedure. It is straight-forward to show that

$$H_{P,I} = \frac{P}{I} = -H_{M1,P} \frac{2j \sin(k\Delta)}{\sqrt{H'_{M2,M1} H_{M1,M2}} - e^{jk\Delta}} e^{-j(\phi + k x_{M1})}, \qquad (2)$$

where $'$ represents the quantity associated with the swapped microphone measurement, $H_{A,B}$ represents the transfer function between A and B, k the wavenumber, $j = \sqrt{-1}$ and Δ the microphone separation, which is 80 mm in the present study. The phase ϕ and the position of M1 (x_{M1}) are unknown constants, but they will not affect the foregoing discussions as far as $|H_{P,I}|$ is the concern. One can also use Eq. (1) to estimate the incident sound/excitation level I as $H_{M1,M1}$ can readily be calculated. The incident sound I presented in the foregoing analysis is the total sound intensity level over the active bandwidth of the mufflers in decibel.

The real time pressure signals from M1 to M4 and P were simultaneously recorded using a Brüel & Kjær Type 3506D PULSE system with a sampling rate of 4096 sample per second per channel. The flow speed U in the present study was varied from 0 m/s to 20 m/s in intervals of 2 m/s. In addition, two artificial acoustic excitation levels were adopted.

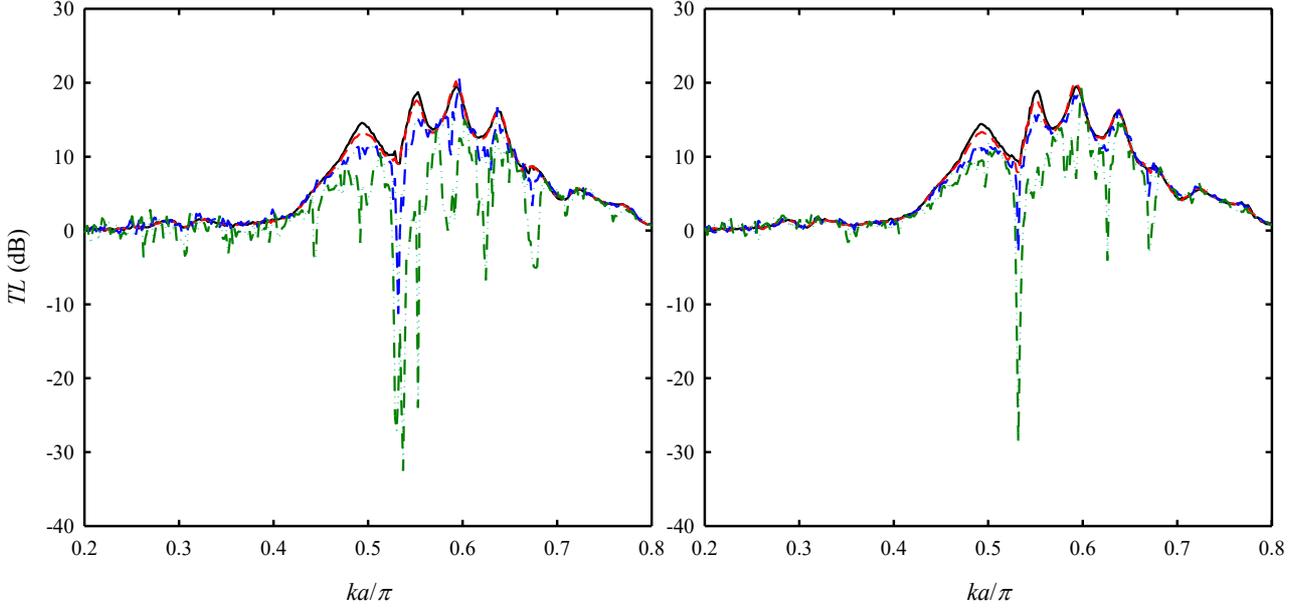FIG. 2   (Color online) Sound transmission loss across the LF muffler.
(a) $I = 103$ dB; (b) $I = 109$ dB.
————— : $U = 0$ m/s; – – – – : $U = 4$ m/s; —·— : $U = 10$ m/s; —··— : $U = 16$ m/s.

III. RESULTS AND DISCUSSIONS

In this section, the effects of flow and the artificial excitation levels on the sound transmission losses (*TL*) across the present sidebranch array muffler are discussed in the first place. The pressure fluctuations within the sidebranches are then examined and a theoretical proposal is developed for reducing the aerodynamic influence on the acoustical performance of the mufflers. The proposal is validated by further experiments.

A. Effects of flow and excitation level on TL

Broadband *TL* can be achieved by the LF sidebranch array muffler when there is no air flow along the duct as shown in Fig. 2. This has been presented in Tang[4] and thus is not further discussed here. The introduction of the low Mach number flow results in a reduction of *TL*. As in many previous studies, such as Tang[21] and Pan et al.,[22] the *TL* reduction is relatively small at low flow speed. The *TL* reduction increases quickly once U exceeds a certain limit (Fig. 2a). At $U = 10$ m/s, the reduction is basically not uniform across the working bandwidth of the muffler and dips can be found at a number of discrete frequencies. A strong sound amplification (negative *TL*) is observed at $ka = 0.5318\pi$. As U increases further to 16 m/s, there are several strong prominent sound amplifications at ka around 0.5318π, while the magnitudes of the other *TL* dips/sound amplifications

8

also increase but at a less rapid pace. Judging from the frequencies of these *TL* dips or sound amplifications, one can conclude that they are due to flow excitation of sidebranches #2 to #7. This will be further discussed later. The shear layer excitation of a sidebranch is a well known aeroacoustical phenomenon, which has been thoroughly reviewed by Tonon et al.[19] However, one should note that the sidebranches in the present study are excited simultaneously by an artificial acoustical excitation as well as the shear layers at their mouths. The interaction between these intervening forces should play a crucial role in shaping the overall aeroacoustical responses. This interaction has not been thoroughly explored at least to the knowledge of the authors.

As there are two forces affecting the sound transmission loss across the present muffler, their relative strength is therefore of great importance in the present study. Figure 2b illustrates the *TL*s across the LF muffler at a higher excitation level of 109 dB. One can notice that the *TL* reduction under a stronger artificial excitation is lower than that under a weaker excitation (Fig. 2a) for the same *U*, except for $U = 0$ m/s where the *TL* is not affected by the acoustic excitation level. The *TL* dip frequencies basically remain unchanged under a stronger artificial acoustic excitation. When *U* is kept constant, the shear rates at the mouths of the sidebranches are more-or-less unchanged and so do the velocity fluctuations created by the shear flows. The stronger *I* results in stronger resonant acoustic velocities near to the mouth of the sidebranches and thus the effect of the flow excitation becomes less significant. The acoustic pressure fluctuation within each sidebranch is also stronger under a higher *I*. A lower *TL* reduction at higher *I* is thus very reasonable.

In order to confirm the above intuition, a single pressure transducer is used to measure the pressure fluctuations along the vertical centrelines of all the sidebranches. The spatial variations of the $\left| H_{P,I} \right|$ spectra within the active sidebranches (#1 to #8) responsible for the strong broadband *TL* of the LF muffler in the 'no flow' case at $I = 103$ dB are presented in Fig. 3. There are low and high pressure regions inside the sidebranches. The strong pressure regions are found at the rigid ends of the sidebranches, which is a typical resonance pattern. It is noticed that the *TL* peaks (Fig. 2a) are usually associated with some relatively strong resonances within different sidebranch combinations.
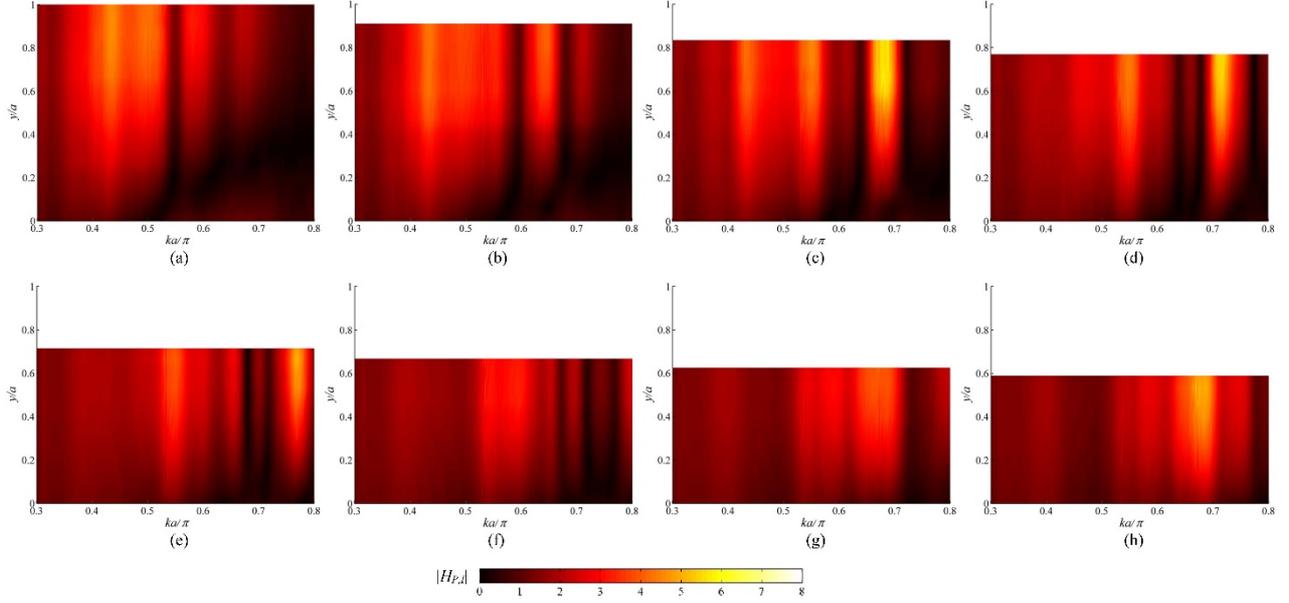
FIG. 3 (Color online) $|H_{P,I}|$ spectra within major active sidebranches of the 11-sidebanch LF muffler.
$U = 0$ m/s, $I = 103$ dB.
(a) #1; (b) #2; (c) #3; (d) #4; (e) #5; (f) #6; (g) #7; (h) #8.

The first *TL* peak at $ka \sim 0.49\pi$ is associated with the coupled resonance between sidebranches #1 and #2. Sidebranches #3 to #5 should be responsible for the second *TL* peak at $ka \sim 0.55\pi$. The third *TL* peak is found at $ka \sim 0.60\pi$, which is related to the relatively stronger acoustical activities inside sidebranches #5 to #7 and the last *TL* peak at $ka \sim 0.64\pi$, should come from the coupled resonance of sidebranches #7, #8 and could be even #9 (not shown here). One can also notice from Fig. 3 that there are strong pressures at $ka \sim 0.68\pi$ inside many sidebranches. However, the corresponding *TL* is not high and thus these pressures are not further discussed until a flow is introduced into the duct.

The corresponding results at $I = 109$ dB are the nearly same as those presented in Fig. 3 and thus they are not presented. One should note that this implies the acoustic pressure fluctuations inside the sidebranches at this excitation level are also stronger than those at $I = 103$ dB in general. Owing to the tube-like structure of the sidebranch, a weak acoustic pressure fluctuation near the mouth of a resonating sidebranch shown in Fig. 3 implies a strong velocity fluctuation there.

In order to understand how the flow modifies the pressures inside the sidebranches and how these modifications have affected the *TL*, the results at $U = 16$ m/s are used as an illustration because the flow-induced noise in this case should be very strong and the effects can be more obviously seen
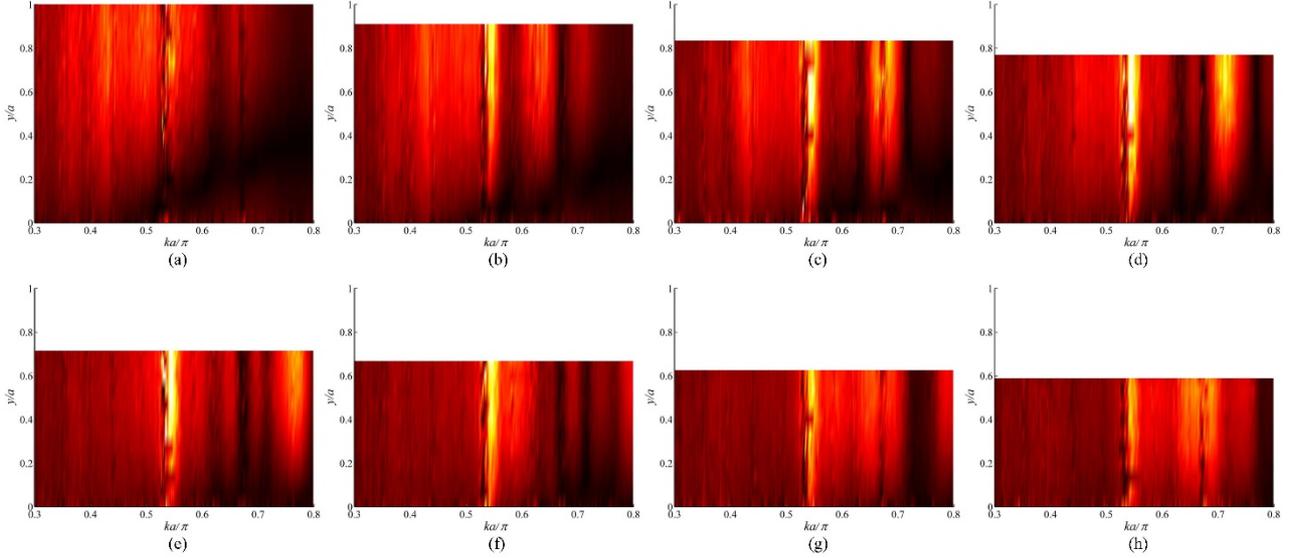
10

FIG. 4 (Color online) Effects of flow on the $|H_{P,I}|$ spectra within major active sidebranches of the 11-sidebanch LF muffler. $U = 16$ m/s, $I = 103$ dB.
(a) #1; (b) #2; (c) #3; (d) #4; (e) #5; (f) #6; (g) #7; (h) #8.
Colour scale : same as that of Fig. 3.

(Fig. 2a). The corresponding $|H_{P,I}|$ spectra are given in Fig. 4. One can notice that the introduction of the flow gives rise to a strong resonance within the muffler at $ka \sim 0.55\pi$, and the worst affected sidebranches are sidebranches #3 to #6. This flow-induced resonance is responsible for the strong sound amplification between $ka \sim 0.53\pi$ to 0.55π (Fig. 2a). The $|H_{P,I}|$ spectra have also become more discrete and thus some of the acoustical couplings between sidebranches at $U = 0$ m/s are seriously disturbed. Strong sound amplification can also be found at $ka \sim 0.44\pi$, 0.49π, 0.62π and 0.68π at $U = 16$ m/s. Most of these sound amplifications are associated with sidebranch pressures of lower magnitudes than those of the 'no flow' case. A clear example of such dip is that at $ka \sim 0.68\pi$ when one compares Figs. 4c, 4g and 4h with Figs. 3c, 3g and 3h respectively. One should bear in mind that the present shear layers are under the moderation of the artificial acoustic excitation and thus are phased locked with the latter.[28] The above observation is thus independent of the position of the sound source relative to the muffler.

Figure 5 shows some typical $|H_{P,I}|$ spectral distributions at $I = 109$ dB with U kept at 16 m/s. In general, the $|H_{P,I}|$ spectra resemble those at $U = 0$ m/s, though a strong flow-induced sound is still observed at $ka \sim 0.55\pi$ and some sound cancellation at $ka \sim 0.68\pi$. However, it is observed that
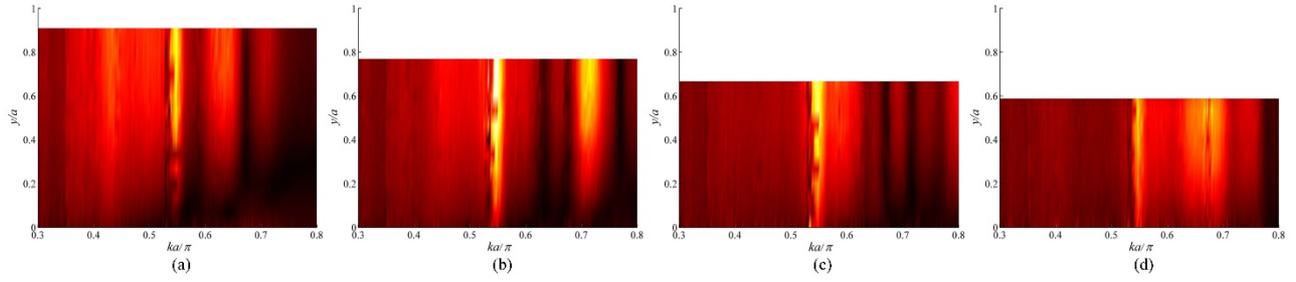
FIG. 5 (Color online) Combined effects of flow and increased artificial excitation on the $|H_{P,I}|$ spectra of the 11-sidebranch LF muffler.
$U = 16$ m/s, $I = 109$ dB.
(a) #2; (b) #4; (c) #6; (d) #8.
Colour scale : same as that of Fig. 3.

1

2   the magnitude of such flow-induced sound is slightly reduced under a stronger I. The original

3   acoustical couplings between sidebranches at $U = 0$ m/s are less disturbed by the flow in the present

4   case of stronger sidebranch internal acoustic pressures than in the case of weaker I (Fig. 4). Thus,

5   the corresponding TL spectrum is closer to that of the 'no flow' case (Fig. 2b).

6   Figures 3 to 5 confirm that stronger pressure fluctuations within the sidebranches can help

7   the LF muffler resist the influence of aerodynamic excitation and thus improve its performance in

8   the presence of a duct flow. Similar phenomena are observed in the case of the LL muffler, and some

9   examples of the corresponding TL spectra are given in Fig. 6 for the sake of completeness. For the

10   LL muffler, the TL dips/sound amplifications grow more rapidly when U is increased beyond 10 m/s
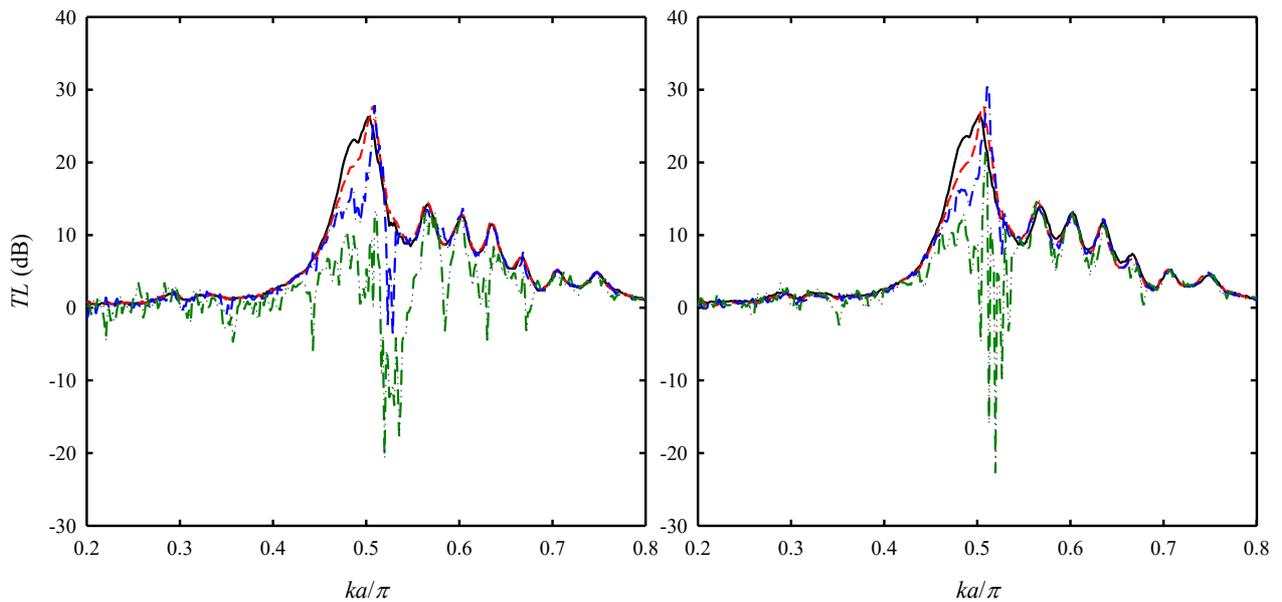
11   under a weaker excitation I.

FIG. 6 (Color online) Sound transmission loss across the LL muffler.
(a) $I = 103$ dB; (b) $I = 109$ dB.
Legends : same as those of Fig. 2.

12

1   In practice, the level of excitation and the flow rate in the duct are usually given as design

2   parameters, a passive method to strengthen the acoustical pressure fluctuations inside the active

3   sidebranches will be very helpful and is discussed in Sections III.B and III.C.

4   **B. A method to reduce flow influence**

5   It can be shown using plane wave propagation theory that a stronger acoustical velocity

6   fluctuation at the mouth of a sidebranch implies a stronger pressure fluctuation within the

7   sidebranch.[29] One can thus expect a stronger resilience of the muffler to aerodynamic excitation

8   according to the results presented in Section III.A (Figs. 3 to 5). In order to seek for a passive method

9   to improve such resilience, the factors affecting these velocity fluctuations have to be made clear.

10   Theoretically, the approach of Huang[30] and Tang[4] can help approximate these velocities in closed

11   forms, but to solve these velocities for an 11-sidebranch muffler analytically is basically not feasible.

12   In this section, a 2-sidebranch muffler is adopted for illustration purpose and the mouths of the

13   sidebranches are treated as massless pistons.

14   Let suffices 1 and 2 denote hereinafter quantity associated with the first and second

15   sidebranch respectively and following the above experimental setup, $l_1 > l_2$ and we set $l_1 = a$ and $l_2 =$

16    $0.95a$. Without loss of generality, $x/a = 0$ represents the axial location of the centerline of the first

17   sidebranch. Denoting the ambient speed of sound by c_0, the acoustical velocities v at the mouths of

18   the sidebranches for the 'no duct flow' case can be obtained by solving the following equation :[4,30]

19
$$\begin{pmatrix} \alpha_1 & \beta \\ \beta & \alpha_2 \end{pmatrix} \begin{pmatrix} v_1 \\ v_2 \end{pmatrix} = \begin{pmatrix} J_1 \\ J_2 \end{pmatrix}, \tag{3}$$

20   where the sidebranch mouth excitation by the propagating plane wave of magnitude I is

21
$$J_i = I \frac{\sin(kw/2)}{kw/2} e^{-jk(i-1)(w+\delta)}, \tag{4a}$$

22
$$\beta = -\frac{\rho c_0}{ka} \left[\frac{\sin^2\left(\frac{kw}{2}\right)}{\frac{kw}{2}} e^{-jkw} + 2j \sum_{m=1}^{\infty} c_m^2 \frac{\sinh^2\left(\frac{kw}{2c_m}\right)}{\frac{kw}{2c_m}} e^{-\left(\frac{kw}{c_m}\right)} \right] \tag{4b}$$

23   where $c_m = \left| \frac{k}{\sqrt{k^2 - (m\pi/a)^2}} \right|$, and

1

$$\alpha_i = j\rho c_0 \cot(kl_i) + j\frac{\rho c_0}{ka}\left\{\left[1 - e^{-j\frac{kw}{2}}\frac{\sin\left(\frac{kw}{2}\right)}{\frac{kw}{2}}\right] - 2\sum_{m=1}^{\infty} c_m^2\left[1 - e^{-\frac{kw}{2c_m}}\frac{\sinh\left(\frac{kw}{2c_m}\right)}{\frac{kw}{2c_m}}\right]\right\}. \quad (4c)$$

2   One obtains

3

$$v_1 = \frac{\alpha_2 J_1 - \beta J_2}{\alpha_1\alpha_2 - \beta^2} \text{ and } v_2 = \frac{\alpha_1 J_2 - \beta J_1}{\alpha_1\alpha_2 - \beta^2}. \quad (5)$$

4   For the sake of easy presentation in the foregoing analysis, the denominator in Eq. (5), which is the

5   same for both v_1 and v_2, will be denoted by G. The second term on the right-hand-side of Eq. (4c),

6   which is the fluid loading and is the same for the two sidebranches, will be represented by F. One

7   should note that β, which represents the mutual induction between the sidebranches, is also the same

8   for the two sidebranches. The magnitudes of v_1 and v_2 are the foci. Expanding Eq. (5), one obtains

9

$$|v_1| = \left|\frac{I}{\rho c_0}\frac{\sin(kw/2)}{kw/2}\right|\left|\frac{\left(F - \beta e^{-jk(w+\delta)}\right)/(\rho c_0) + j\cot(kl_2)}{G/(\rho c_0)^2}\right|$$

and

$$|v_2| = \left|\frac{I}{\rho c_0}\frac{\sin(kw/2)}{kw/2}\right|\left|\frac{\left(F - \beta e^{jk(w+\delta)}\right)/(\rho c_0) + j\cot(kl_1)}{G/(\rho c_0)^2}\right|. \quad (6)$$

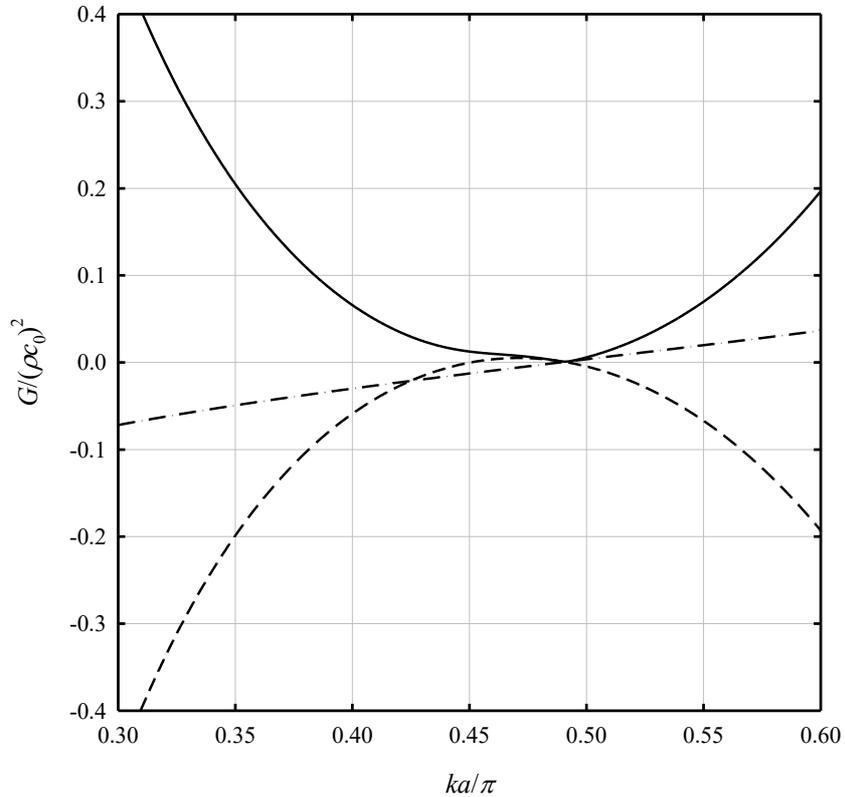10   In the calculations of G and F, 2000 modes are included in summation series.

FIG. 7 Spectral variation of G of the 2-sidebranch muffler.
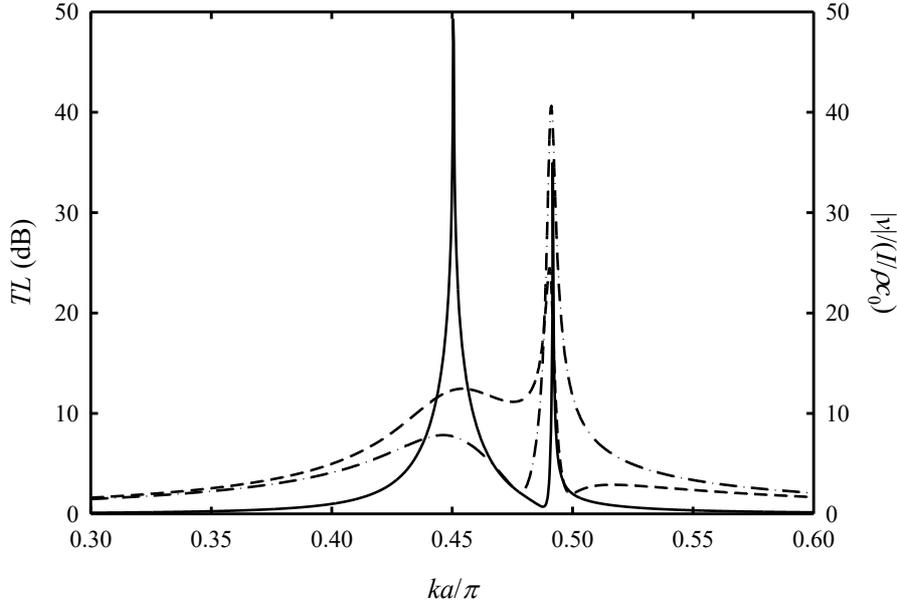———— : $|G|$; – – – – : Re(G); —·—— : Im(G).

FIG. 8 Spectral variations of *TL* and branch mouth velocity magnitudes of
the 2-sidebranch muffler.
———— : *TL*; – – – – : |v_1|; — · — : |v_2|.

1 The active bandwidth of this two-sidebranch muffler is defined mainly by *G* whose magnitude

2 varies substantially over the frequency range of interest. |*G*| is in general small for $0.44 < ka/\pi < 0.50$

3 and is the smallest at $ka/\pi \sim 0.49$ where Im(*G*) vanishes (Fig. 7). The latter represents the resonance

4 frequency the coupled system formed by the sidebranches and the main duct. The magnitudes of the

5 acoustical velocities are the highest around this frequency as shown in Fig. 8. There are two *TL*

6 peaks; one at $ka/\pi \sim 0.49$ and the other at $ka/\pi \sim 0.45$ (Fig. 8). The former is that due to the

7 abovementioned resonance effect. The latter takes place around the frequency where Re(*G*) vanishes.

8 The relatively higher acoustical velocities there should be the result of the nominators in Eq. (5), and

9 thus those in the second terms of the right-hand-side of Eq. (6).

10 Figure 9a shows the spectral variations of the various components that make up the

11 nominators within the frequency range of significant *TL*. One can notice from Fig. 9a that the

12 sidebranch impedances $j\cot(kl)$ are counteracting the imaginary parts of $(F - \beta e^{\pm jk(w+\delta)})/\rho c_0$

13 throughout the concerned frequency range. An obvious method to increase the mouth velocity

14 magnitude of second sidebranch in this frequency range is to have $(F - \beta e^{jk(w+\delta)})/\rho c_0$ to interact with

15 $j\cot(kl_2)$ instead of $j\cot(kl_1)$. The situation of the first sidebranch is less straight-forward. In principle,

16 the nominator magnitude may increase if $(F - \beta e^{-jk(w+\delta)})/\rho c_0$ is counteracted by a less positive
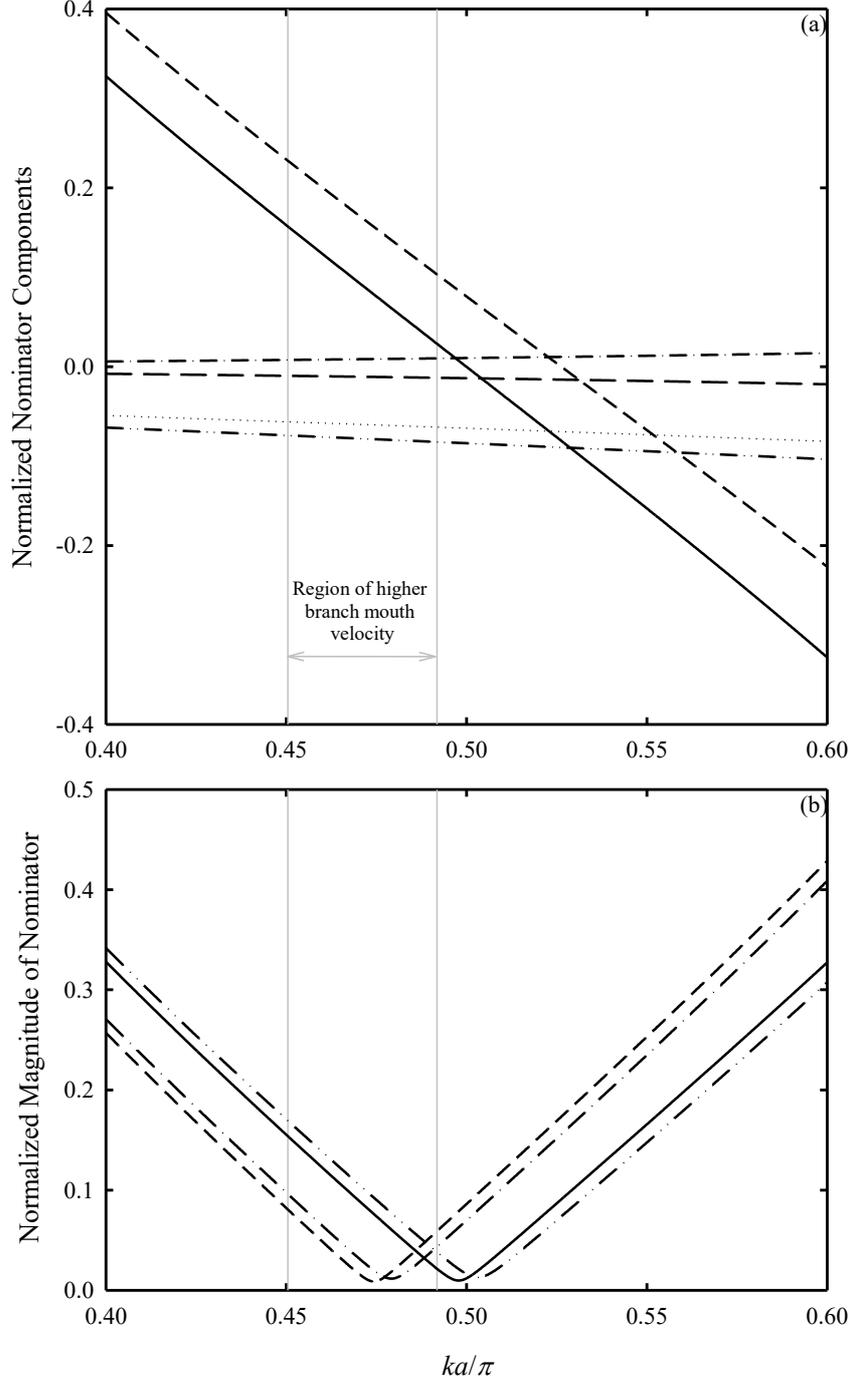
15

FIG. 9 (a) Spectral variations of the components in the nominators of Eq. 6 within the strong *TL* frequency range of the 2-sidebranch muffler.
———— : $\cot(kl_1)$; – – – – : $\cot(kl_2)$;
— · — : $\mathrm{Re}(F - \beta e^{-jk(w+\delta)})/\rho c_0$; — ·· — : $\mathrm{Im}(F - \beta e^{-jk(w+\delta)})/\rho c_0$;
— — : $\mathrm{Re}(F - \beta e^{jk(w+\delta)})/\rho c_0$; ········ : $\mathrm{Im}(F - \beta e^{jk(w+\delta)})/\rho c_0$;
(b) Magnitudes of the nominators before and after swapping the impedance terms.
———— : $|(F - \beta e^{-jk(w+\delta)})/\rho c_0 + j\cot(kl_2)|$; – – – – : $|(F - \beta e^{-jk(w+\delta)})/\rho c_0 + j\cot(kl_1)|$;
— · — : $|(F - \beta e^{jk(w+\delta)})/\rho c_0 + j\cot(kl_1)|$; — ·· — : $|(F - \beta e^{jk(w+\delta)})/\rho c_0 + j\cot(kl_2)|$.

1   impedance term within the frequency range in which the sum of $(F - \beta e^{-jk(w+\delta)})/\rho c_0$ and the impedance

2   term has a negative imaginary part. An obvious choice to achieve this is to replace the impedance

3   term $j\cot(kl_2)$ by $j\cot(kl_1)$ in Eq. (6) for v_1, though it works only for a narrow bandwidth.
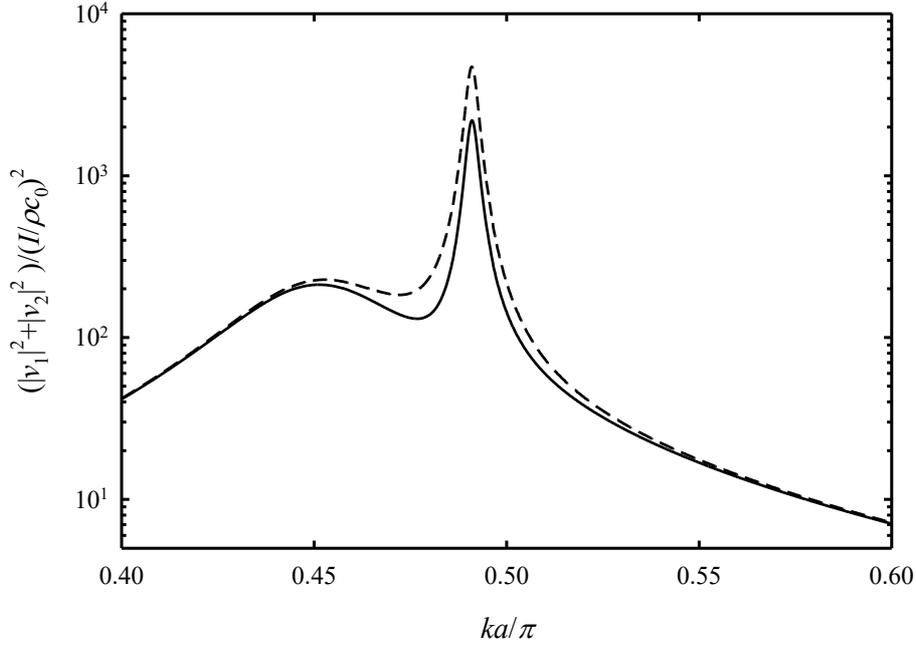
FIG. 10   Overall kinetic energy of air at the mouths of the 2-sidebranch mufflers
              before and after swapping impedance.
              ———— : $l_1 = a$, $l_2 = 0.95a$; – – – – : $l_1 = 0.95a$, $l_2 = a$.

1   Figure 9b illustrates the magnitudes of the nominators in Eq. (6) under the abovementioned

2   combinations between fluid loading, mutual induction and sidebranch impedance. As discussed

3   above, the magnitude of the velocity at the mouth of second sidebranch over nearly the entire active

4   bandwidth is increased by replacing $j\cot(kl_1)$ by $j\cot(kl_2)$ in Eq. (6). There is a reduction in the

5   velocity magnitude at the mouth of the first sidebranch for $ka < 0.485\pi$. However, since $|G|$ is very

6   small as $ka \to 0.49\pi$, the increase in corresponding velocity magnitude is very strong at $ka > 0.485\pi$.

7   Outside the active frequency range of the muffler, the magnitude of G increases quickly. The mouth

8   velocities are then weak and eventually become insignificant. Figure 10 illustrates the increase in

9   the overall kinetic energy of air at the sidebranch mouths after swapping the impedance terms in Eq.

10   (6). One can also notice from the same equation that the swapping of impedance terms is equivalent

11   to reversing the order of the sidebranches.

12   The TL across the muffler section can be approximated according to Tang :[4]

13
$$TL = -20\log_{10}\left|1 + \frac{\rho c_0}{ka}\sin\left(\frac{kw}{2}\right)\sum_{i=1}^{2}\frac{v_i}{I}e^{jk(i-1)(w+\delta)}\right|$$

17

$$= -20\log_{10}\left|1 + \frac{2\rho c_0}{ka}\frac{\sin^2\left(\frac{kw}{2}\right)}{kw}\left(\frac{2F - 2\beta\cos[k(w+\delta)] + j\rho c_0\sum_{m=1}^{2}\cot(kl_i)}{G}\right)\right|, \quad (7)$$

which is independent of the sidebranch order in the 2-sidebranch muffler for the 'no flow' case, though the sidebranch order does affect the acoustic pressure and particle velocities within the sidebranches as shown in Fig. 9b.

The above treatment has been repeated using a 3-sidebranch LL muffler. However, the solutions are very lengthy and tedious, but the conclusions are the same and thus the corresponding results are not presented. It is expected that the above concept works in general for narrow sidebranch array mufflers.

C. Experimental validation

The analysis in Section III.B is an approximation, and thus the corresponding conclusions need validation. Experiments in Section III.A with both LL and LF mufflers are repeated with the order of the siderbanches reversed and corresponding results will be discussed in this section. The letter 'R' is added next to LL and LF hereinafter to denote the case where the original sidebranch order is reversed.

Figures 11a to 11d illustrate the distributions of $|H_{P,I}|$s inside some sidebranches of the 11-sidebranch LFR muffler at $U = 0$ m/s, $I = 103$ dB. By comparing them with Figs. 3b, 3d, 3f and 3h, one can notice that the acoustic pressures inside this LFR muffler are much stronger than those in the corresponding LF muffler, though they are excited at the same artificial acoustic excitation level. The resonances are more distinctly seen in the LFR muffler. This agrees with the theoretical deduction using the 2-sidebranch muffler in Section III.B.

The introduction of a flow of $U = 16$ m/s at $I = 103$ dB does disturb slightly the $|H_{P,I}|$ spectra as shown in Figs. 11e to 11h, but the changes are much weaker than those observed inside the corresponding LF muffler. Increasing I to 109 dB with U kept at 16 m/s results in very small change in the $|H_{P,I}|$ maps (Figs. 11i to 11l) compared to those at $I = 103$ dB. In fact, these maps are closer to those at $I = 103$ dB of the 'no flow' case. The stronger acoustic pressures inside the sidebranches
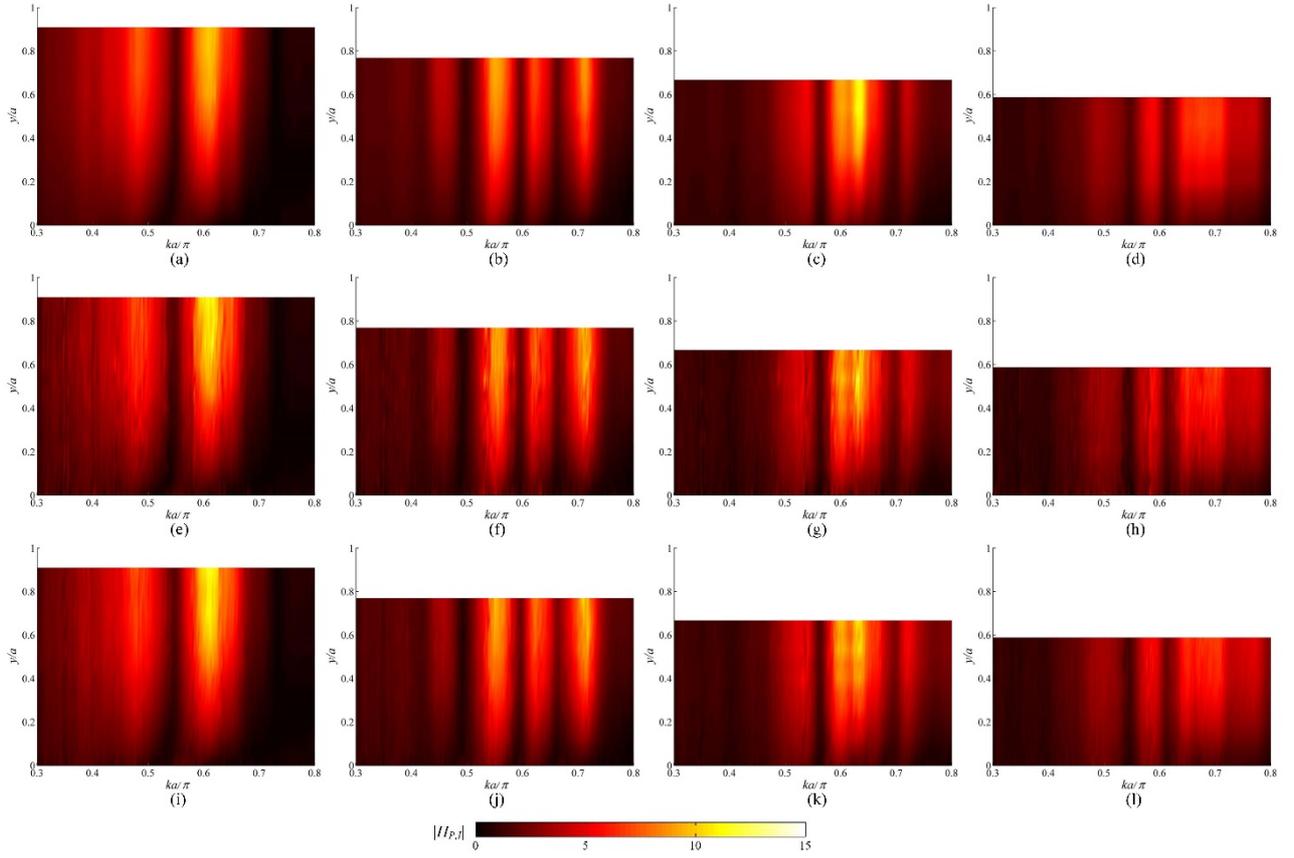
18

FIG. 11   (Color online) Examples of $|H_{P,I}|$ spectra of the 11-sidebanch LFR muffler.
$U = 0$ m/s, $I = 103$ dB : (a) #2; (b) #4; (c) #6; (d) #8;
$U = 16$ m/s, $I = 103$ dB : (e) #2; (f) #4; (g) #6; (h) #8;
$U = 16$ m/s, $I = 109$ dB : (i) #2; (j) #4; (k) #6; (l) #8.

1   after reversing the order of the sidebranches improves the resilience of the muffler to aerodynamic

2   disturbance.

3   The spectral variations of the *TL*s across the LFR and LLR mufflers are presented in Fig. 12.

4   The *TL*s of the LFR mufflers in the 'no flow' case are more-or-less similar to that of the original LF

5   muffler (Figs. 2 and 6). This agrees with the deduction of Eq. (7) though this equation is developed

6   using a muffler consists of two sidebranches. At $I = 103$ dB, the *TL* of the LFR muffler are higher

7   than those of the original LF muffler under the same flow speed (Fig. 12a). Though, there are still

8   *TL* dips when U exceeds 10 m/s, their magnitudes are very much reduced, showing that the strong

9   air pressure under the reversed sidebranch arrangement has helped lowering down the effect of flow

10   induced pressure fluctuations which are detrimental to the acoustical performance of the muffler.

11   Same applies to the case of the LLR muffler as shown in Fig. 12b. For the case of the LLR muffler,

12   the improvement of *TL* is impressive at high flow speed of $U = 16$ m/s where nearly no negative *TL*

13   is found within the active bandwidth of the muffler. The *TL*s of the reversed mufflers are further
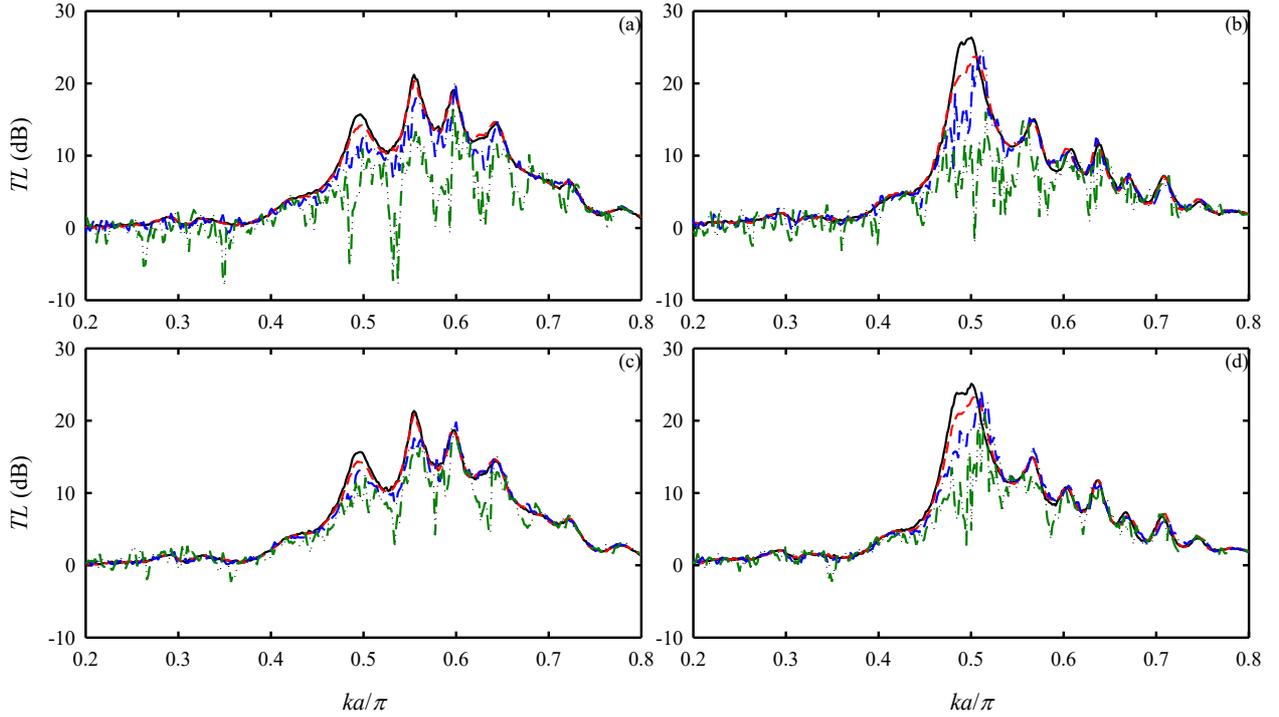
FIG. 12   (Color online) Sound transmission losses across mufflers with sidebranch order reversed.
(a) LFR muffler, $I = 103$ dB; (b) LLR muffler, $I = 103$ dB;
(c) LFR muffler, $I = 109$ dB; (d) LLR muffler, $I = 109$ dB.
————— : $U = 0$ m/s; – – – – : $U = 4$ m/s; — · — : $U = 10$ m/s; — ·· — : $U = 16$ m/s.

1   improved as I increases (Figs. 12c and 12d). This is rather expected and thus the corresponding

2   results are not further discussed.

3   The present results show that it is possible to improve the resilience of sidebranch array

4   muffler to flow excitation by arranging them in the order of decreasing branch mouth impedance

5   magnitude. It is believed that such concept can also be applied to flow duct silencing devices formed

6   by coupling reactive elements.

7

8   **IV. CONCLUSIONS**

9   The sound transmission loss across a duct muffler formed by eleven closely packed narrow

10   sidebranches arranged in the form of a linear array is investigated experimentally in the present study.

11   The lengths of the sidebranches decrease along the length of the muffler. The effects of a low Mach

12   number duct flow on the acoustical performance of the muffler are also examined. A passive method

13   to improve the resilience of this type of muffler against aerodynamic disturbance is also developed

14   theoretically and validated by experiments.

In the absence of a duct flow, the sidebranch array muffler can offer impressive broadband sound transmission loss. The introduction of a low Mach number flow lowers down its performance. At a fixed upstream acoustic excitation level, the increase in the flow velocity results in more serious performance deterioration. Strong sound transmission loss dips are observed at high flow velocity. At a fixed duct flow velocity, a stronger upstream excitation improves the sound transmission loss of the muffler. Stronger sound pressures inside the sidebranches help maintain muffler acoustical performance.

A stronger acoustic velocity at the mouth of a sidebranch implies stronger acoustic pressure fluctuations within the sidebranch. A theoretical analysis is then carried out in order to understand how the fluid loading, branch impedance and mutual induction between sidebranches are affecting the mouth air velocity. A two-sidebranch muffler is adopted for illustration as it is amenable to analytical solution. It is found that putting the shorter sidebranch (stronger acoustic impedance magnitude) upstream of the longer one will increase the total kinetic energy of the air at the mouths of the sidebranches, resulting in stronger sound pressures inside the sidebranches.

Further experiment is conducted with the order of the sidebranches in the original muffler is reversed. Results show that the acoustical performance of the muffler in the presence of a duct flow can be improved after the reversion, validating the theoretical deduction obtained using the two-sidebranch muffler. It is expected that such concept can be applied to other duct silencing devices formed by coupling reactive elements. The present finding also suggests that the mouth impedances of these elements have to be considered during their optimization for flow duct applications. It is also believed that the elements should be arranged in the order of decreasing impedance magnitude to minimize aerodynamic influences.

[1] A. Fry, *Noise Control in Building Services* (Pergamon, Oxford, 1988), Chap. 7.

[2] L. L. Beranek, "Criteria for office quieting based on questionnaire rating studies," J. Acoust. Soc. Am. **28**, 833 – 852 (1956).

[3] L. L. Beranek and I. L. Vér, *Noise and Vibration Control Engineering : Principles and Applications* (Wiley, New York, 1992), Chap. 10.

[4] S. K. Tang, "Narrow sidebranch arrays for low frequency duct noise control," J. Acoust. Soc. Am. **132**, 3086 – 3097 (2012).

[5] L. Huang and Y. S. Choy, "Vibro-acoustics of three dimensional drum silencer," J. Acoust. Soc. Am. **118**, 2313 – 2320 (2005).

[6] S. Allam and M. Åbom, "A new type of muffler based on microperforated tubes," Trans. ASME : J. Vib. Acoust. **133**, 031005 (2011).

[7] G. Canevet, "Active sound absorption in an air conditioning duct," J. Sound Vib. **58**, 333 – 345 (1978).

[8] U. Ingard, "On the theory and design of acoustic resonators," J. Acoust. Soc. Am. **25**, 1037 – 1061 (1953).

[9] J. G. Ih, "Reactive attenuation of rectangular plenum chambers," J. Sound Vib. **157**, 93 – 122 (1992).

[10] A. Salemat, N. S. Dickey, and J. M. Novak, "The Herschel-Quincke tube: A theoretical, computational and experimental investigation," J. Acoust. Soc. Am. **96**, 3177 – 3185 (1994).

[11] C. Q. Howard, R. A. Craig, "Noise reduction using a quarter wave tube with different orifice geometries," Appl. Acoust. **76**, 180 – 186 (2014).

[12] M. L. Munjal, *Acoustics of Ducts and Mufflers with Application to Exhaust and Ventilation System Design* (Wiley, New York, 1987).

[13] Y. J. Tang and S. K. Tang, "On low frequency sound propagation across closely coupled narrow cavities along an infinite duct and the similarity in stopband cut-on frequencies," J. Sound Vib. **443**, 411 – 429 (2019).

[14] D. P. Jena and X. J. Qiu, "Sound transmission loss of porous materials in ducts with embedded periodic scatterers," J. Acoust. Soc. Am. **147**, 978 – 983 (2020).

[15] S. Griffin, S. A. Lane and S. Huybrechts, "Coupled Helmholtz resonators for acoustic attenuation," Trans. ASME, J. Vib. Acoust. **123**, 11 – 17 (2001).

[16] S. H. Seo and Y. H. Kim, "Silencer design using array resonators for low frequency band noise reduction," J. Acoust. Soc. Am. **118**, 2332 – 2338 (2005).

[17] C. Q. Howard, B. S. Cazzolato, and C. H. Hansen, "Exhaust stack silencer design using finite element analysis," Noise Control Eng. J. **48**, 113 – 120 (2000).

[18] M. Červenka and M. Bednařík, "Optimal reactive silencers with narrow side-branch tubes," J. Acoust. Soc. Am. **144**, 2015 – 2021 (2018).

[19] D. Tonon, A. Hirschberg, J. Golliard and S. Ziada, "Aeroacoustics of pipe systems with closed branches," Int. J. Aeroacoust. **10**, 201 – 276 (2011).

[20] P. A. Nelson, N. A. Halliwell and P. E. Doak, "Fluid dynamics of a flow-excited resonance, Part I : Experiment," J. Sound Vib. **78**, 15 – 38 (1981).

[21] S. K. Tang, "On sound transmission loss across Helmholtz resonator in a low Mach number flow duct," J. Acoust. Soc. Am. **127**, 3519 – 3525 (2010).

[22] W. Pan, X. Xu, J. Li and Y. Guan, "Acoustic damping performance of coupled Helmholtz resonators with a sharable perforated sidewall in the presence of grazing flow," Aero. Sci. Tech, **99**, 105573 (2020).

[23] H. M. Yu and S. K. Tang, "Low frequency interactions between coupled narrow sidebranch arrays and the resulted sound transmission loss," Appl. Acoust. **117**, 51 – 60 (2017).

[24] W. Neise, W. Frommhold, F. P. Mechel and F. Holste, "Sound power determination in rectangular flow ducts," J. Sound Vib. **174**, 201 – 237 (1994).

[25] S. K. Tang and F. Y. C. Li, "On low frequency sound transmission loss of double sidebranches: A comparison between theory and experiment," J. Acoust. Soc. Am. **113**, 3215 – 3225 (2003).

[26] J. Y. Chung and D. A. Blaser, "Transfer function method of measuring in-duct acoustic properties. I. Theory," J. Acoust. Soc. Am. **68**, 907 – 913 (1980).

[27] M. Åbom and H. Bodén, "Error analysis of two-microphone measurements in ducts with flow," J. Acoust. Soc. Am. **83**, 2429 – 2438 (1988).

[28] A. K. M. F. Hussain, "Coherent structures and turbulence," J. Fluid Mech. **173**, 303 – 356 (1986).

[29] L. E. Kinsler, A. R. Frey, A. B. Coppens and J. V. Sanders, *Fundamentals of Acoustics*, 4th ed. (Wiley, New York, 2000), Chap. 10.

[30] L. Huang, "A theory of reactive control of low-frequency duct noise," J. Sound Vib. **238**, 575 – 594 (2000).

1		Captions
2	Figure 1	Schematics of the experimental setup and cross-section of sidebranch muffler.
3		All dimensions in mm.
4	Figure 2	(Color online) Sound transmission loss across the LF muffler.
5		(a) $I = 103$ dB; (b) $I = 109$ dB.
6		———— : $U = 0$ m/s; $----$: $U = 4$ m/s; —·— : $U = 10$ m/s; —··— : $U = 16$ m/s.
7	Figure 3	(Color online) $\lvert H_{P,I} \rvert$ spectra within major active sidebranches of the 11-sidebanch
8		LF muffler.
9		$U = 0$ m/s, $I = 103$ dB.
10		(a) #1; (b) #2; (c) #3; (d) #4; (e) #5; (f) #6; (g) #7; (h) #8.
11	Figure 4	(Color online) Effects of flow on the $\lvert H_{P,I} \rvert$ spectra within major active sidebranches
12		of the 11-sidebanch LF muffler. $U = 16$ m/s, $I = 103$ dB.
13		(a) #1; (b) #2; (c) #3; (d) #4; (e) #5; (f) #6; (g) #7; (h) #8.
14		Colour scale : same as that of Fig. 3.
15	Figure 5	(Color online) Combined effects of flow and increased artificial excitation on the
16		$\lvert H_{P,I} \rvert$ spectra of the 11-sidebranch LF muffler. $U = 16$ m/s, $I = 109$ dB.
17		(a) #2; (b) #4; (c) #6; (d) #8.
18		Colour scale : same as that of Fig. 3.
19	Figure 6	(Color online) Sound transmission loss across the LL muffler.
20		(a) $I = 103$ dB; (b) $I = 109$ dB.
21		Legends : same as those of Fig. 2.
22	Figure 7	Spectral variation of G of the 2-sidebranch muffler.
23		———— : $\lvert G \rvert$; $----$: Re(G); —·— : Im(G).
24	Figure 8	Spectral variations of TL and branch mouth velocity magnitudes of the 2-sidebranch
25		muffler.
26		———— : TL; $----$: $\lvert v_1 \rvert$; —·— : $\lvert v_2 \rvert$.

1 Figure 9   (a) Spectral variations of the components in the nominators of Eq. 6 within the strong

2   TL frequency range of the 2-sidebranch muffler.

3   ——— : $\cot(kl_1)$; $-\ -\ -\ -$: $\cot(kl_2)$;

4   — · — : $\mathrm{Re}(F - \beta e^{-jk(w+\delta)})/\rho c_0$; — ·· — : $\mathrm{Im}(F - \beta e^{-jk(w+\delta)})/\rho c_0$;

5   — — : $\mathrm{Re}(F - \beta e^{jk(w+\delta)})/\rho c_0$; ········· : $\mathrm{Im}(F - \beta e^{jk(w+\delta)})/\rho c_0$;

6   (b) Magnitudes of the nominators before and after swapping the impedance terms.

7   ——— : $|(F - \beta e^{-jk(w+\delta)})/\rho c_0 + j\cot(kl_2)|$; $-\ -\ -\ -$: $|(F - \beta e^{-jk(w+\delta)})/\rho c_0 + j\cot(kl_1)|$;

8   — · — : $|(F - \beta e^{jk(w+\delta)})/\rho c_0 + j\cot(kl_1)|$; — ·· — : $|(F - \beta e^{jk(w+\delta)})/\rho c_0 + j\cot(kl_2)|$.

9 Figure 10   Overall kinetic energy of air at the mouths of the 2-sidebranch mufflers before and

10   after swapping impedance.

11   ——— : $l_1 = a$, $l_2 = 0.95a$; $-\ -\ -\ -$: $l_1 = 0.95a$, $l_2 = a$.

12 Figure 11   (Color online) Examples of $|H_{P,I}|$ spectra of the 11-sidebanch LFR muffler.

13            $U = 0$ m/s, $I = 103$ dB : (a) #2; (b) #4; (c) #6; (d) #8;

14            $U = 16$ m/s, $I = 103$ dB : (e) #2; (f) #4; (g) #6; (h) #8;

15            $U = 16$ m/s, $I = 109$ dB : (i) #2; (j) #4; (k) #6; (l) #8.

16 Figure 12   (Color online) Sound transmission losses across mufflers with sidebranch order

17   reversed.

18   (a) LFR muffler, $I = 103$ dB; (b) LLR muffler, $I = 103$ dB;

19   (c) LFR muffler, $I = 109$ dB; (d) LLR muffler, $I = 109$ dB.

20   ——— : $U = 0$ m/s; $-\ -\ -\ -$: $U = 4$ m/s; — · — : $U = 10$ m/s; — ·· — : $U = 16$ m/s.

21